JOURNAL OF SOLID STATE CHEMISTRY **131,** 387–393 (1997)
ARTICLE NO. SC977408

A Lamellar Hydrated Barium Cobalt Phosphate with a Two-Dimensional Array of Co–O–Co Network: $Ba(CoPO_4)_2 \cdot H_2O$

Xianhui Bu, Pingyun Feng, and Galen D. Stucky

Department of Chemistry, University of California, Santa Barbara, California 93106

Received February 6, 1997; in revised form March 31, 1997; accepted April 2, 1997

The hydrothermal synthesis and X-ray crystal structure of a hydrated barium cobalt phosphate are presented. The structure is built from cobalt octahedra edge-shared with phosphorus tetrahedra. Cobalt polyhedra form corner-sharing chains along the crystallographic *b* axis. These chains are interconnected by water molecules and phosphate groups to form an infinite two-dimensional sheet. Sheets are stacked along the crystallographic *c* axis with charge balancing cations, Ba^{2+}, located in the interlayer region. The structure also consists of two-dimensional arrays of Co–O–Co networks with cobalt centers forming hexagonal patterns. There are a limited number of cobalt(II) phosphates in which the Co/P ratio is 1. A summary of these cobalt(II) phosphates is given. A classification scheme based on the extent of the Co–O–Co linkage is provided for cobalt phosphates. Crystal data for $Ba(CoPO_4)_2 \cdot H_2O$, $M = 463.16$, space group $C2$ (No. 5), $a = 9.2494(4)$ Å, $b = 4.9140(2)$ Å, $c = 8.2650(4)$ Å, $\beta = 91.744(2)^\circ$, $V = 375.48(3)$ Å^3, $Z = 2$, $D_c = 4.097$ g cm^{-3}, thin plate, Mo$K\alpha$, $\lambda = 0.71073$ Å, $\mu = 10.005$ mm^{-1}, $2\theta_{max} = 56.44^\circ$, $R(F) = 2.43\%$ for 70 parameters and 908 reflections with $I > 2\sigma(I)$.

INTRODUCTION

Divalent metal phosphates (MPO_4^-, $M = Be^{2+}$, Zn^{2+}, Co^{2+} …) are of interest for a number of reasons, one of which is that they can form zeolite-like framework structures (1). Zeolites are aluminosilicates with uniformly sized cages and channels and are used for a variety of commercial applications such as heterogeneous catalysis, ion exchange, and adsorption (2). The incorporation of transition metals into the framework sites opens up more possible applications for zeolitic materials, especially as shape-selective redox catalysts (3). We have previously reported a number of zinc phosphates with novel framework structures, two of which possess a framework topology derived from that of sodalite (4–6). We found that the charge matching between the host framework and guest species is an important factor in the condensation of the inorganic framework. More recently, we have synthesized and characterized a family of cobalt phosphates containing monovalent cations (Na^+, K^+, Rb^+, and NH_4^+) as extra-framework charge balancing species (7–9). The structures of these cobalt phosphates are related to that of the zeolite ABW type. In order to make a zeolite-like tetrahedral cobalt phosphate, a ratio of 1 between Co and P is required. We found that the size of the extra-framework inorganic cations plays an important role in determining the framework structure type of these cobalt phosphates. We have now extended our exploratory synthesis to include cobalt phosphates with alkaline-earth metals as extra framework species in order to further study the effect of cation size and charge matching. Another stimulus for the study of cobalt phosphates is the interesting magnetic properties they may possess and the sensitivity of their magnetic properties to the coordination environment. Here, we report the synthesis, crystal structure of the first hydrated cobalt phosphate containing an alkaline-earth metal.

EXPERIMENTAL

Hydrothermal Synthesis and Initial Characterizations

$CoCl_2 \cdot 6H_2O$ (1.18 g) was mixed with 10.4 g of distilled water. A total of 0.97 g of 85% H_3PO_4 was slowly added to the above mixture. After stirring, 0.86 g of $Ba(OH)_2 \cdot 8H_2O$ was added. The pH of the solution was adjusted with 1.50 g of 40% CH_3NH_2 to a value of 10.47 as measured using a Ag/AgCl electrode pH meter. The whole mixture was stirred for 1 h and then heated at 160°C for 3 days in a Teflon-coated steel autoclave. The product was recovered by filtration and washed with deionized water.

The microscopic examination indicates that the product is a mixture of two or more phases. The phase described here consists of very small plate-like crystals with the largest dimension less than 100 μm. The color of the crystals is dark red or light blue depending on the orientation of the crystals with respect to the viewing direction. All X-ray powder diffraction peaks could be indexed with the unit cell parameters for the phase reported here. This indicates that the unknown phase(s) might be amorphous.

A total of 49.8 mg of the as-synthesized sample was used in thermogravimetric analysis (TGA) and differential

0022-4596/97 $25.00

thermal analysis (DTA) which were performed on a Netzsch simultaneous thermal analysis (STA) 409 system in static air with a heating rate of 5°C/min from 30 to 1000°C. Between 30 and 300°C, there was a continuous weight decrease with a total loss of 5.2%. However, between 380 and 440°C there was one sharp peak for a weight loss of 1.9% accompanied by a prominent endothermic peak. The latter is believed to be from the phase described here. Since the calculated weight loss for the title compound is 3.9%, the TGA result suggests that the about 50 wt% of the as-synthesized sample is the phase described here.

Single-Crystal Structure Determination

A crystal was glued to a thin glass fiber with epoxy resin and mounted on a Siemens Smart CCD diffractometer equipped with a normal focus, 2.4 KW sealed tube X-ray source (Mo$K\alpha$ radiation, $\lambda = 0.71073$ Å) operating at 50 kV and 40 mA. A full sphere of intensity data was collected in 2082 frames with ω scans (width of 0.30° and exposure time of 30 sec per frame). Unit cell dimensions were determined by a least-squares fit of 1832 reflections with $I > 10\sigma(I)$. The empirical absorption correction was based on the equivalent reflections and other possible effects such as the absorption by the glass fiber were simultaneously corrected. The structure was solved by Patterson methods followed by successive difference Fourier methods. All calculations were performed using SHELXTL running on Silicon Graphics Indy 5000. Final full-matrix refinements were against F^2 with all reflections and included secondary extinction correction and anisotropic thermal parameters for all non-hydrogen atoms. The hydrogen atom was located from the difference Fourier and refined isotropically. The crystallographic results are summarized in Table 1, while the atomic coordinates, selected bond distances, and angles are listed in Tables 2 and 3, respectively.

TABLE 1
Summary of Crystal Data and Refinement Results

Structural formula	$Ba(CoPO_4)_2 \cdot H_2O$
Formula weight	463.16
Crystal size (μm^3)	$93 \times 33 \times 27$
a (Å)	9.2494(4)
b (Å)	4.9140(2)
c (A)	8.2650(4)
β (°)	91.744(2)
V (Å^3)	375.48 (3)
Z	2
Space group	$C2$ (No. 5)
ρ_{calc} (g/cm^3)	4.097
λ (Mo$K\alpha$) (Å)	0.71073
μ(Mo$K\alpha$) (mm^{-1})	10.005
Maximum 2θ	56.44°
Unique data $I > 2\sigma(I)$	895
Parameters	70
$R(F)^a$	2.43%
$R_w(F^2)^b$	6.26%
GOF	1.044

$^aR(F) = \sum||F_o| - |F_c||/\sum|F_o|$ with $F_o > 4.0\ \sigma(F)$.
$^bR_w(F^2) = [\sum[w(F_o^2 - F_c^2)^2]/\sum[w(F_o^2)^2]]^{1/2}$ with $F_o > 4.0\sigma(F)$. $w = 1/[\sigma^2(F_o^2) + (0.0446P)^2 + 0.7694P]$, where $P = (F_o^2 + 2F_c^2)/3$.

TABLE 2
Atomic Coordinates ($\times 10^4$) and Equivalent Isotropic Displacement Parameters (Å$^2 \times 10^3$)

	x	y	z	U_{eq}
Ba(1)	5000	7258	5000	11(1)
Co(1)	1670(1)	6631(2)	1495(1)	9(1)
P(1)	3457(1)	2318(4)	2388(1)	9(1)
O(1)	0	3790(16)	0	24(2)
O(2)	1801(5)	8544(8)	− 668(5)	13(1)
O(3)	5044(4)	2839(9)	2921(5)	14(1)
O(4)	2439(4)	3963(9)	3440(5)	14(1)
O(5)	3186(4)	9277(9)	2481(5)	12(1)
H(1)	421(94)	3091(207)	− 446(112)	33(29)

Note. U_{eq} is defined as one third of the trace of the orthogonalized U_{ij} tensor.

TABLE 3
Selected Bond Lengths (Å) and Angles (°)

Ba(1)–O(4)#1	2.763(4)	Ba(1)–O(4)#2	2.763(4)
Ba(1)–O(3)#3	2.770(4)	Ba(1)–O(3)	2.770(4)
Ba(1)–O(5)#3	2.815(4)	Ba(1)–O(5)	2.815(4)
Ba(1)–O(4)#3	3.116(4)	Ba(1)–O(4)	3.116(4)
Ba(1)–O(3)#4	3.237(4)	Ba(1)–O(3)#5	3.237(4)
Co(1)–O(2)	2.027(4)	Co(1)–O(3)#6	2.027(4)
Co(1)–O(5)	2.061(4)	Co(1)–O(4)	2.177(5)
Co(1)–O(2)#7	2.197(4)	Co(1)–O(1)	2.397(5)
P(1)–O(5)#8	1.518(5)	P(1)–O(4)	1.531(4)
P(1)–O(3)	1.541(4)	P(1)–O(2)#7	1.555(4)
O(2)–Co(1)–O(3)#6	116.2(2)	O(2)–Co(1)–O(5)	89.9(2)
O(3)#6–Co(1)–O(5)	95.3(2)	O(2)–Co(1)–O(4)	154.6(2)
O(3)#6–Co(1)–O(4)	88.8(2)	O(5)–Co(1)–O(4)	83.4(2)
O(2)–Co(1)–O(2)#7	89.39(10)	O(3)#6–Co(1)–O(2)#7	151.5(2)
O(5)–Co(1)–O(2)#7	97.0(2)	O(4)–Co(1)–O(2)#7	67.3(2)
O(2)–Co(1)–O(1)	82.5(2)	O(3)#6–Co(1)–O(1)	89.56(12)
O(5)–Co(1)–O(1)	172.2(2)	O(4)–Co(1)–O(1)	102.8(2)
O(2)#7–Co(1)–O(1)	81.3(2)	O(5)#8–P(1)–O(4)	112.7(2)
O(5)#8–P(1)–O(3)	107.9(2)	O(4)–P(1)–O(3)	110.3(2)
O(5)#8–P(1)–O(2)#7	114.0(2)	O(4)–P(1)–O(2)#7	103.6(3)
O(3)–P(1)–O(2)#7	108.4(2)	Co(1)#9–O(1)–Co(1)	108.8(3)
P(1)#10–O(2)–Co(1)	127.9(2)	P(1)#10–O(2)–Co(1)#10	93.8(2)
Co(1)–O(2)–Co(1)#10	130.6(2)	P(1)–O(3)–Co(1)#11	120.1(2)
P(1)–O(4)–Co(1)	95.2(2)	P(1)#5–O(5)–Co(1)	135.5(3)

Symmetry transformations used to generate equivalent atoms:

#1 $-x+1/2, y+1/2, -z+1$	#2 $x+1/2, y+1/2, z$	#3 $-x+1, y, -z+1$
#4 $-x+1, y+1, -z+1$	#5 $x, y+1, z$	#6 $x-1/2, y+1/2, z$
#7 $-x+1/2, y-1/2, -z$	#8 $x, y-1, z$	#9 $-x, y, -z$
#10 $-x+1/2, y+1/2, -z$	#11 $x+1/2, y-1/2, z$	#12 $x-1/2, y-1/2, z$

RESULTS AND DISCUSSION

Description of Local Coordination Features

An interesting structural feature is the edge sharing between the P tetrahedron and the Co octahedron (Fig. 1). The Co^{2+} ion adopts slightly distorted octahedral coordination, whereas the P^{5+} is tetrahedrally coordinated as usual. In many of divalent metal phosphates (MPO_4^-, $M = Be^{2+}$, Zn^{2+}, Co^{2+} ...), it is rather common to form edge-sharing polyhedra between metal centers with low valence. However, edge sharing with the highly charged P^{5+} tetrahedra shortens the distance between cationic polyhedral centers compared to corner sharing and thus creates unfavorable electrostatic repulsion. As a result, such a structural feature is not very common. Another example of Co and P as edge-sharing polyhedra is found in a related lamellar compound, $Sr(CoPO_4)_2$ (10).

Another notable structural feature is the presence of the Co–O–Co linkages. The occurrence of metal–oxygen–metal linkages is not an unusual feature among divalent metal phosphates (MPO_4^-, $M = Be^{2+}$, Zn^{2+}, Co^{2+} ...). Such a feature is in general associated with relatively dense materials and does not exist in materials which can be considered as zeolite like. However, the presence of the Co–O–Co linkages has an important effect in the magnetic properties of these metal phosphates. There are two different types of Co–O–Co linkages in the title compound based on the coordination environment of the bridging oxygen atoms. In the first type, the bridging oxygen atom is also part of phosphorus tetrahedra. This type of Co–O–Co linkage is commonly found in other divalent metal phosphates (MPO_4^-, $M = Be^{2+}$, Zn^{2+}, Co^{2+} ...) as well. In the second type, the bridging oxygen is a water molecule. This type of bridging is less common. It should be noted that water molecules in two related salts, $Co(HPO_4)\cdot H_2O$ and $NH_4CoPO_4\cdot H_2O$, are pendant molecules on the octahedral Co^{2+} centers (11, 12).

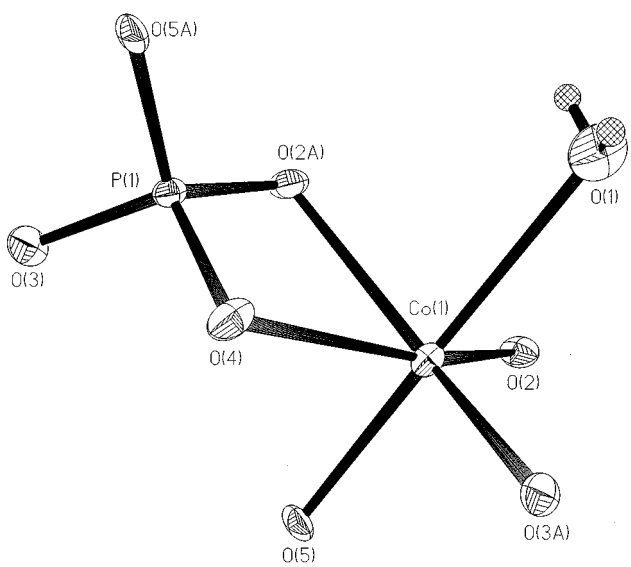

FIG. 1. An ORTEP (50%) drawing showing the local coordination environment. O1 is the water molecule. O2 is trigonally coordinated between two Co atoms and one P atom. O3, O4 and O5 are bicoordinated between one Co atom and one P atom (excluding the possible coordination to extra-framework Ba atoms). Atoms with labels containing "A" are symmetry generated. The asymmetric unit is $Ba_{1/2}(CoPO_4)(H_2O)_{1/2}$, suggesting that the Ba cation and the H_2O molecule are located on the 2-fold axis.

Stoichiometry and Cobalt Phosphates with a Co/P Ratio of 1

The local coordination sphere surrounding each polyhedral center determines the ratio between the number of different polyhedral centers and the overall stoichiometry of the compound. To derive the Co/P ratio from a certain type of connectivity, it is necessary to consider the nearest coordination from one type of polyhedral center to the other type. The ratio between the two polyhedral centers is the reciprocal ratio of the number of connectivity of the two polyhedral centers. Here, the number of connectivity of one polyhedral center is defined as the number of the other type of polyhedral atoms connected to it through oxygen bridges and may not be the same as the coordination number. We have used this concept in the analysis of several other polymeric structures (13–15). In some cases, it is easier to consider a cluster of oxygen polyhedral centers as a single unit and analyze the ratio between different clusters. Such an understanding of polymeric structures may help in the future design of new polymeric phases.

As a result of the Co–O–Co linkage and the edge sharing between Co^{2+} octahedra and P^{5+} tetrahedra in the title compound, each Co^{2+} cation is connected to only four phosphorus cations through the oxygen bridges and each phosphorus center is connected to four Co^{2+} centers (Fig. 2). This gives rise to a ratio of 1 for Co/P. There are a very limited number of cobalt(II) phosphates in which the Co/P ratio is 1. Since such a stoichiometry is a prerequisite in synthesizing cobalt phosphate zeolite analogs with alternating Co and P tetrahedra and is of considerable interest in this regard, all known cobalt(II) phosphates in the ICSD (16) with a Co/P ratio of 1 are tabulated in Table 1 together with a brief description of structural features.

The change of the cobalt phosphate framework with the increasing cation size from Na^+ to NH_4^+ and Rb^+ has been discussed in detail previously (9). The adoption of the olivine structural type, rather than phenacite, quartz, or cristobalite type by $LiCoPO_4$ (17, 18), agrees with the observation we made previously: $CoPO_4$ frameworks can more easily accommodate smaller ions by increasing the coordination number and thus the overall framework

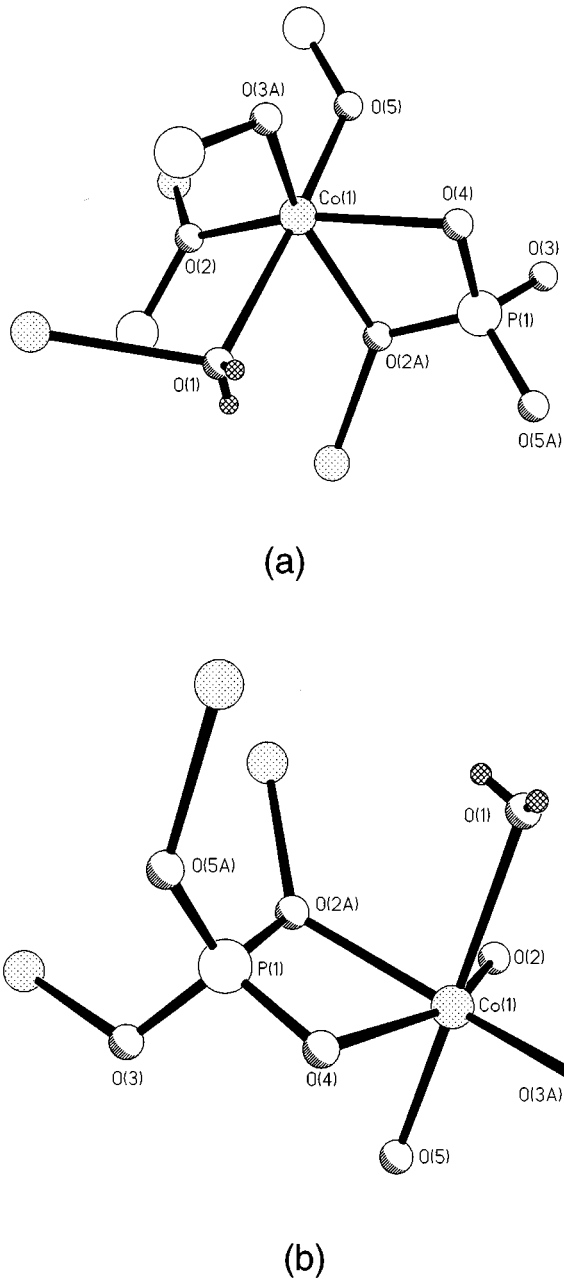

FIG. 2. (a) An octahedral Co^{2+} connected to four P^{5+} tetrahedra through oxygen atoms; (b) A tetrahedral P^{5+} connected to four Co^{2+} octahedra through oxygen atoms.

density than by changing the tetrahedral framework structure into a different topology (9). In this study, we note that cobalt phosphates with relatively large cations such as $Sr(CoPO_4)_2$ and the title compound have a lamellar structure (10, 12). This may indicate a tendency to form lamellar structures for large inorganic cations.

Description of the Connectivity within the Polymeric Layer

The title compound consists of negatively charged layers of $CoPO_4 \cdot H_2O$ stacked along the crystallographic c axis, the length of which is the interlayer spacing. The charge of the inorganic polymeric sheet, $(CoPO_4 \cdot H_2O)_n^{n-}$ is neutralized by counterions, Ba^{2+}, located in the interlayer region. To understand the connectivity within the polymeric layer, we first examine how the Co–O–Co linkages are joined into an infinite array. If we do not consider the coordination of Co^{2+} to the water molecule and phosphate groups, an infinite chain of corner sharing Co^{2+} polyhedra propagating along the crystallographic b axis (the polar direction) is obtained (Fig. 3). Multiple, parallel chains are arranged along the a axis separated by half of the a axial length. The water molecule serves as a bidentate ligand that bridges the Co chains in a rather simple way as depicted in Fig. 4. The phosphate has a slightly complicated bridging style as shown in Fig. 5. Through the oxygen atoms, each P cation connects to one Co^{2+} in one chain and to three other Co centers in the other chain. So the polymeric layer can be considered as built from parallel corner-sharing cobalt chains bridged by water molecules and phosphate groups.

Classification of Cobalt Phosphates Based on Co–O–Co Linkages

The magnetic properties of cobalt phosphates are intimately related to the structural connectivity of constituent atoms. The magnetic coupling between two adjacent cobalt centers in cobalt phosphates can be either through –O–P–O– bridges or –O– bridges. In general, the coupling through the phosphate groups is fairly weak and is seldom observed beyond 3 K (9). Thus, at temperatures higher than 3 K, the magnetic coupling in cobalt phosphate salts is mostly through Co–O–Co linkages. We have been especially interested in the various ways in which Co–O–Co linkages join together in cobalt phosphate salts and have chosen to classify cobalt phosphates into five classes. It should be noted that such a classification is based on the bonding patterns of cobalt and oxygen atoms only. The first class consists of isolated cobalt polyhedra and no Co–O–Co

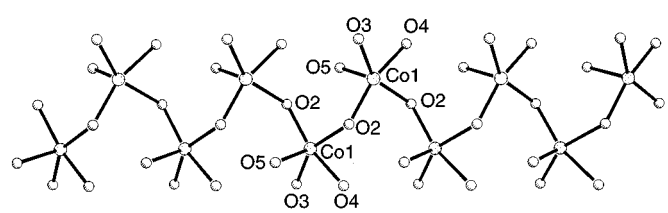

FIG. 3. A corner-sharing Co^{2+} chain along the crystallographic b axis.

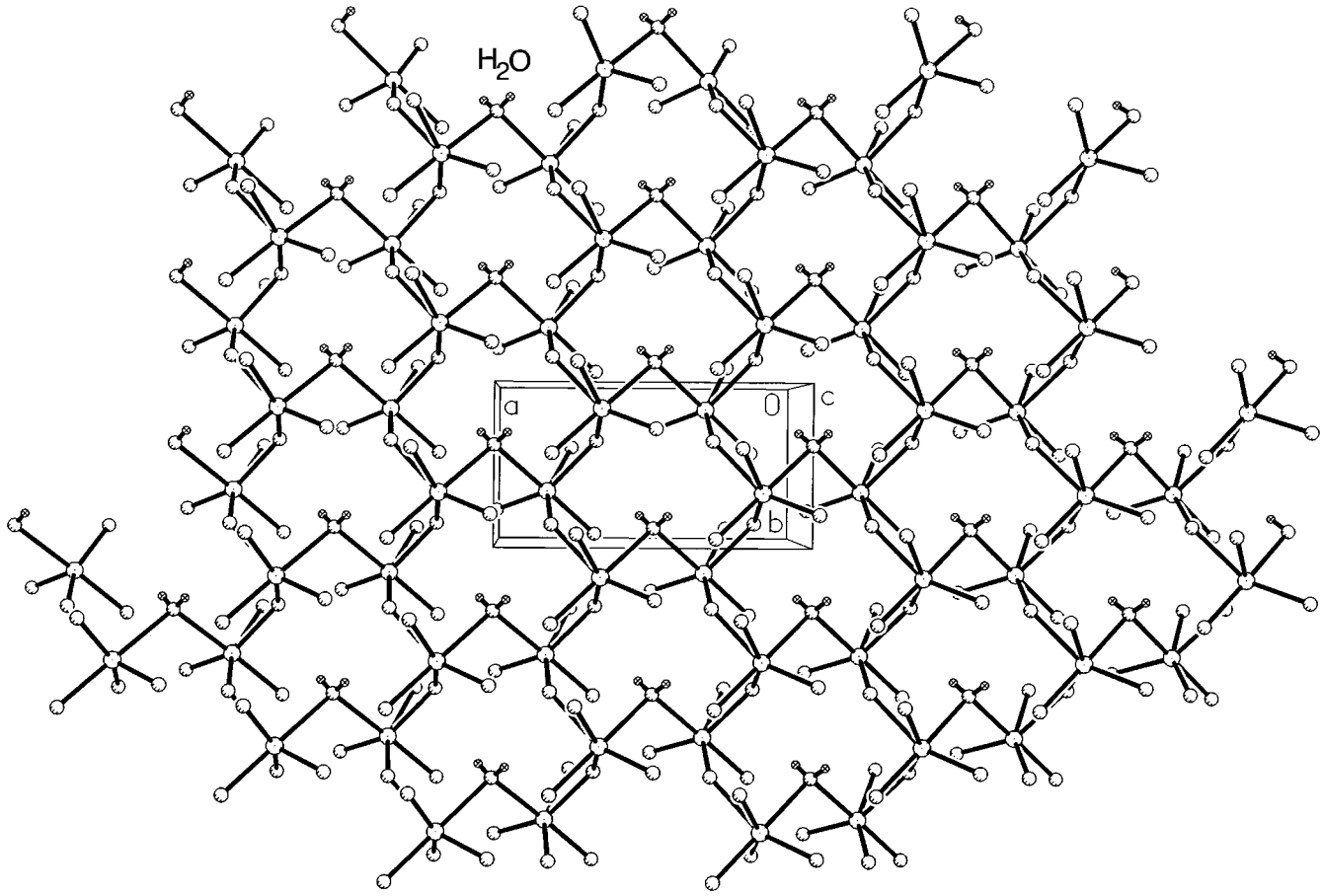

FIG. 4. A two-dimensional network of Co–O–Co linkages formed through the cross linking of corner-sharing Co chains. The chains are linked together by phosphate groups (P^{5+} is omitted) and water molecules.

linkages. These salts include a family of recently discovered zeolite-like cobalt phosphates, $MCoPO_4$ ($M = Na^+$, K^+, NH_4^+, Rb^+) (9). The absence of Co–O–Co linkages usually favors the formation of relatively less dense structures and is thus a desired feature in the synthesis of zeolite-like cobalt phosphates. However, the magnetic behavior of these materials is usually paramagnetic down to 3 K.

In the second class, there are finite clusters of Co–O–Co linkages. One example is the red polymorph of $NaCoPO_4$ which consists of the cobalt oxygen cluster with four cobalt ions (7). In the third class, there are infinite one-dimensional chains of Co–O–Co linkages. The pink polymorph of $NaCoPO_4$ is one such example (8). It consists of an infinite linear edge-sharing Co octahedra. In the fourth class, there are two-dimensional arrays of Co–O–Co linkages. In addition to the title compound, infinite two-dimensional arrays are also observed in $LiCoPO_4$ and $NH_4CoPO_4 \cdot H_2O$ (12). In the latter two compounds, each cobalt is 4-connected within the layer to form a pattern similar to that of a distorted chessboard with each ring consisting of four cobalt ions. This is in contrast with the title compound in which each cobalt is 3-connected within the layer such that each ring in the hexagonal layer consists of six cobalt ions (Fig. 4).

In the fifth class, there is a three-dimensional array of Co–O–Co linkages. The three-dimensional array of the Co–O–Co network is found in cobalt oxides such as CoO which has a NaCl, zinc blende or Wurtzite structure (19) and Co_3O_4 which has a spinel structure (20). However, no cobalt phosphate with a Co/P ratio of 1 has been found to have a three-dimensional array of Co–O–Co linkages (Table 4). Based on the above analysis on the relationship between the stoichiometry and the connectivity, cobalt phosphates with a Co/P ratio of 1 (or less) are unlikely to form a three-dimensional array of Co–O–Co linkages. The relative amount of cobalt increases with the formation of 3-D Co–O–Co network, whereas the phosphorus is unable to increase its relative amount to the same level as that of the

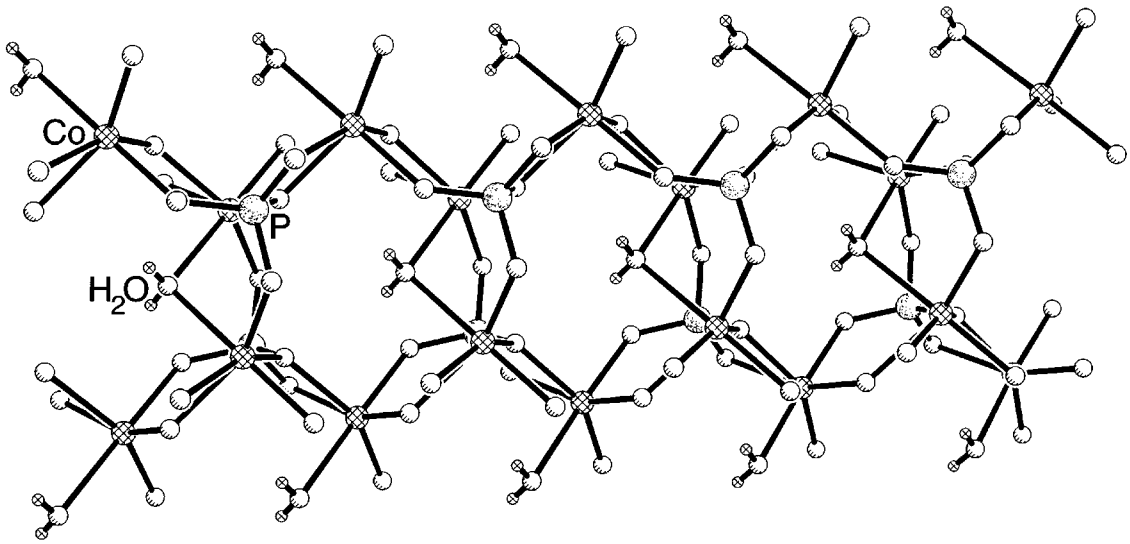

FIG. 5. Two Co^{2+} chains cross linked by phosphate groups and water molecules.

cobalt (other that through the formation of P–O–P linkages in pyrophosphates which we consider to be a different class of materials.). Thus, in cobalt phosphates, such a structural feature will be limited to those with a Co/P ratio higher than 1 such as $Co_2(OH)PO_4$ (21). Since no magnetic properties have been reported for $Co_2(OH)PO_4$, we have performed the magnetic susceptibility measurements on a sample of $Co_2(OH)PO_4$. This material is paramagnetic from room temperature down to 70 K at which a transition into an antiferromagnetic phase occurs. Such a transition temperature is very high compared to that of the two polymorphs of $NaCoPO_4$ (7, 8) which belong to Class 2 (with a transition temperature of 15 K) and Class 3 (with a transition temperature of 13 K), respectively. It is very likely that such a large difference in transition temperatures is mainly related to the differing extent of the Co–O–Co network.

As illustrated above for Class 4 salts ($LiCoPO_4$, $NH_4CoPO_4 \cdot H_2O$, and the title compound), in principle, many different patterns for Co–O–Co linkages could be found for each class. In designing new magnetic or zeolitic materials, control of such structural features should be of

TABLE 4
A Summary of 14 Inorganic Cobalt(II) Phosphate Salts with a Co/P Ratio of 1

Compounds	Co polyhedra	Framework type	Co–O–Co connectivity
$LiCoPO_4$ (18)	Octahedral	Olivine	Infinite 2-D array (4-ring)
$NaCoPO_4$ (9, 22)	Tetrahedral	ABW–tridymite hybrid	Alternating Co, P tetrahedra
$NaCoPO_4$ (7)	5-coordinate	Not classified yet	Finite cluster with 4 Co ions
$NaCoPO_4$ (8, 22)	Octahedral	$ZnSO_4$	Edge-sharing straight chain
$KCoPO_4$ (9)	Tetrahedral	ABW–tridymite hybrid	Alternating Co, P tetrahedra
$RbCoPO_4$ (9)	Tetrahedral	Zeolite ABW	Alternating Co, P tetrahedra
NH_4CoPO_4 (9)	Tetrahedral	Zeolite ABW	Alternating Co, P tetrahedra
NH_4CoPO_4 (9)	Tetrahedral	ABW–tridymite hybrid	Alternating Co, P tetrahedra
$NH_4CoPO_4H_2O$ (12)	Octahedral	Lamellar	Infinite 2-D array (4-ring)
$AgCoPO_4$ (23)	5- and 6-coordinate	Not classified yet	Corner, edge-sharing chain
$Mg(CoPO_4)_2$ (24)	5- and 6-coordinate	γ-$Zn_3(PO_4)_2$	Mg, Co solid solution
$Sr(CoPO_4)_2$ (10)	4- and 5-coordinate	Lamellar	Finite cluster with four Co ions
$Ba(CoPO_4)_2H_2O$	Octahedral	Lamellar	Infinite 2-D array (6-ring)
$Co(HPO_4)H_2O$ (11)	Octahedral	Not classified yet	Edge-sharing helical chain

considerable importance. It is of interest to study these materials and their magnetic properties systematically in order to get a more complete understanding of the structure–property relation for cobalt phosphate salts.

ACKNOWLEDGMENTS

This research was supported in part by the National Science Foundation under Grant DMR 95-20971.

REFERENCES

1. T. E. Gier and G. D. Stucky, *Nature* **349,** 508 (1991).
2 .D. W. Breck, "Zeolite Molecular Sieves." Wiley, New York, 1974.
3. S. S. Lin and H. S. Weng, *Appl. Catal.* **A105,** 289 (1993).
4. X. H. Bu, P. Y. Feng, and G. D. Stucky, *J. Solid State Chem.* **125,** 243 (1996).
5. X. H. Bu, T. E. Gier, and G. D. Stucky, *Acta Crystallogr.* **C52,** 1601 (1996).
6. P. Y. Feng, X. H. Bu, and G. D. Stucky, *Angew. Chem* (*Int. Ed.*) **34,** 1745 (1995).
7. P. Y. Feng, X. H. Bu, and G. D. Stucky, *J. Solid State Chem.* **129,** 328–333 (1997).
8. P. Y. Feng, X. H. Bu, and G. D. Stucky, *J. Solid State Chem.* **131,** 160–166 (1997).
9. P. Y. Feng, X. H. Bu, S. H. Tolbert, and G. D. Stucky, *J. Am. Chem. Soc.* **119,** 2497–2504 (1997).
10. B. Elbali, A. Boukhari, E. M. Holt, and J. Aride, *J. Crystallogr. Spectrosc. Res.* **23,** 1001 (1993).
11. H. Effenberger, R. Parik, F. Pertlik, and B. Rieck, *Z. Kristallogr.* **194,** 199 (1991).
12. D. Tranqui, A. Durif, J. C. Guitel, and M. T. Averbuch-Pouchot, *Bull. Soc. Chim. Fr.* **1968,** 1759 (1968).
13. T. E. Gier, X. H. Bu, S. L. Lein, and G. D. Stucky, *J. Am. Chem. Soc.* **118,** 3039 (1996).
14. X. H. Bu, T. E. Gier, and G. D. Stucky, *Acta Crystallogr.* **C52,** 2662 (1996).
15. P. Y. Feng, X. H. Bu, and G. D. Stucky, *Acta Crystallogr.*, in press.
16. "Inorganic Crystal Structure Database," FIZ Karlsruhe and Gmelin-Institut, 1996.
17. O. Muller and R. Roy, "The Major Ternary Structural Families." Springer-Verlag, New York, 1974.
18. F. Kubel, *Z. Kristallogr.* **209,** 755 (1994).
19. M. J. Redman and E. G. Steward, *Nature* **193,** 867 (1962).
20. W. L. Smith and A. D. Hobson, *Acta Crystallogr.* **B29,** 362 (1973).
21. W. T. A Harrison, J. T. Vaughey, L. L. Dussack, A. J. Jacobson, T. E. Martin, and G. D. Stucky, *J. Solid State Chem.* **114,** 151 (1995).
22. R. Hammond and J. Barbier, *Acta Crystallogr.* **B52,** 440 (1996).
23. I. Tordjman, J. C. Guitel, A. Durif, M. T. Averbuch, and R. Masse, *Mater. Res. Bull.* **13,** 983 (1978).
24. A. G. Nord and T. Stefanidis, *Z. Kristallogr.* **153,** 141 (1980).